Discover Oncology

Case Study

Unraveling the heterogeneity of WHO grade 4 gliomas: insights from clinical, imaging, and molecular characterization

Haihui Jiang[1] · Xijie Wang[2] · Xiaodong Chen[1] · Shouzan Zhang[1] · Qingsen Ren[1] · Mingxiao Li[2] · Ming Li[2] · Xiaohui Ren[2] · Song Lin[2,3] · Yong Cui[2,3]

Received: 13 October 2024 / Accepted: 13 January 2025
Published online: 03 February 2025

Abstract

Purpose The 2021 WHO classification of central nervous system tumors introduced molecular criteria to stratify Grade 4 gliomas, which remain heterogeneous. This study aims to elucidate the clinical, radiological, and molecular characteristics of WHO Grade 4 gliomas, focusing on their prognostic implications and the development of a predictive model for astrocytoma IDH-mutant WHO Grade 4 (A4).

Methods A retrospective cohort of 223 patients from Beijing Tiantan Hospital was analyzed. Clinical, radiological, and histopathological data were combined with molecular profiling, focusing on IDH mutations, TERT promoter mutations, and MGMT methylation. A predictive model was developed using LASSO regression to distinguish A4 from glioblastomas and validated with an external dataset from UCSF.

Results The cohort included 201 glioblastomas (90.1%) and 22 A4 cases (9.9%). A4 tumors were associated with younger age, higher MGMT promoter methylation, lower rates of TERT mutations, and distinct radiological features, such as cortical non-enhancing tumor infiltration (CnCE). Patients with A4 demonstrated significantly better survival outcomes compared to glioblastoma patients ($p < 0.001$). The predictive model for A4, incorporating age, tumor margin, and CnCE, achieved an AUC of 0.890 in the training set and 0.951 in the validation set.

Conclusion Integrating molecular and clinical criteria improves prognostication in Grade 4 gliomas. The predictive model developed in this study effectively identifies A4 tumors, facilitating more personalized therapeutic strategies.

Keywords Molecular pathology · Glioblastoma · WHO CNS 5 · Prognosis · Predictive marker

Abbreviations

IDH	Isocitrate dehydrogenase
TERT	Telomerase reverse transcriptas
EGFR	Epidermal growth factor receptor
BTH	Beijing Tiantan Hospital

Haihui Jiang, Xijie Wang and Xiaodong Chen have contribute equally to this article.

Supplementary Information The online version contains supplementary material available at https://doi.org/10.1007/s12672-025-01811-0.

✉ Song Lin, linsong2005@126.com; ✉ Yong Cui, cuiyong20130422@163.com | [1]Department of Neurosurgery, Peking University Third Hospital, Peking University, Beijing, China. [2]Department of Neurosurgery, Beijing Tiantan Hospital, Capital Medical University, Beijing, China. [3]National Clinical Research Center for Neurological Diseases, Center of Brain Tumor, Beijing Institute for Brain Disorders and Beijing Key Laboratory of Brain Tumor, Beijing, China.

UCSF PDGM	The University of California, San Francisco Preoperative Diffuse Glioma MRI Dataset
EOR	Extent of resection
GTR	Gross-total resection
NTR	Near-total resection
STR	Subtotal resection
A4	Astrocytoma, IDH-mutant, WHO Grade 4
mGBM	Molecular glioblastoma
hGBM	Histologic glioblastoma
SVZ	The subventricular zone
CE	Contrast-enhancing
CnCE	Cortical non-enhancing tumor infiltration
CE/nCE	Ratio of contrast enhancement diameter to non-enhancing tumor diameter
OS	Overall survival
MGMT	O^6-methylguanine-DNA methyltransferase
LASSO	Least absolute shrinkage and selection operator
DCA	Decision curve analysis
ROC	Receiver-operating characteristic
AUC	Area under the curve

1 Introduction

The WHO 2021 classification introduced a novel stratification system for gliomas, delineating distinct subtypes within Grade 4 tumors based on molecular and histological features [1]. Isocitrate dehydrogenase (IDH) wild-type gliomas with the molecular hallmarks of telomerase reverse transcriptase (TERT) promoter mutation, epidermal growth factor receptor (EGFR) amplification, or chromosomes 7 gain 10 loss are now categorized as WHO Grade 4 glioblastomas, irrespective of the histologic features [2]. While IDH-mutant astrocytomas with histologic features of necrosis and/or microvascular proliferation or CDKN2A/B homozygous deletion can be also grouped as WHO Grade 4 [3]. Despite their molecular and histological diversity, Grade 4 gliomas share unfavorable prognostic traits such as rapid recurrence and limited survival. Notably, the classification underscores the prognostic significance of IDH status, with IDH-mutant gliomas generally exhibiting a more favorable clinical course compared to their wild-type counterparts [4]. Previous investigations have consistently demonstrated superior prognoses for IDH-mutant glioblastomas relative to IDH wild-type variants [4–6], prompting the conceptualization of "secondary glioblastomas" evolving from low-grade gliomas harboring IDH mutations [7].

IDH wild-type astrocytomas represent a rare subgroup characterized by heterogeneous clinical and molecular profiles, and dismal prognosis. Previous studies have revealed that the majority of IDH wild-type Grade 2 and Grade 3 astrocytomas exhibit an aggressive clinical course akin to glioblastomas [8–11]. Studies have identified prognostic risk factors such as TERT promoter mutations and EGFR amplification in IDH wild-type Grade 2 astrocytomas, with worse outcomes observed in cases accompanied by EGFR amplification [8]. Despite efforts by the WHO to integrate traditional histological criteria and molecular features of glioblastomas into a biomolecular grading scheme for IDH-wild-type astrocytoma, dissenting opinions exist regarding the prognostic implications of this classification. In a retrospective study, Berzero et al. [12] found that Grade 2 astrocytomas meeting molecular criteria demonstrated a significantly better prognosis than traditionally diagnosed glioblastomas. Giannini et al. [13] argue that isolated TERT mutations in Grade 2 IDH wild-type astrocytomas are insufficient to drive the aggressive clinical progression observed in Grade 4 glioblastomas, as their survival rates far exceed those of glioblastomas.

Historically, IDH mutant astrocytomas with glioblastoma-like histologic features were termed "secondary glioblastomas" and classified as Grade 4 tumors. However, emerging evidence suggests a significantly better prognosis for IDH-mutant glioblastomas compared to their wild-type counterparts, prompting their reclassification as Astrocytoma, IDH-mutant, WHO Grade 4 (A4) [4–6]. Notably, despite this redefinition, these tumors retain their Grade 4 classification. Previous research reported that IDH-mutant astrocytomas with additional adverse molecular alterations, such as CDKN2A/B homozygous deletion, demonstrate a markedly shortened prognosis [6, 14–17]. As a result, these cases are also categorized as A4. Nevertheless, limited research exists on molecularly diagnosed A4, emphasizing the need for further investigation into their clinical and molecular characteristics.

The integration of preoperative neuroimaging and clinical features for predicting IDH status in glioblastoma holds significant clinical value. This approach can facilitate early and informed decision-making by weighing the risks and benefits of surgical and nonsurgical management, given the substantial prognostic differences between IDH-mutant and IDH-wildtype grade 4 malignant gliomas.

In this context, our retrospective analysis of Grade 4 malignant gliomas diagnosed between 2019 and 2021 aims to elucidate their clinical, radiological, and molecular features and to disclose the prognostic implications of different WHO Grade 4 variants. We further validated our findings using the University of California, San Francisco Preoperative Diffuse Glioma MRI Dataset (UCSF PDGM) [18] as an external database. By examining a cohort of 223 cases, we seek to contribute valuable insights that may inform future diagnostic classifications and therapeutic strategies for gliomas.

2 Materials and methods

2.1 Patients and inclusion criteria

The study cohort comprised 223 consecutive patients who underwent surgical intervention for gliomas at the Neurosurgical Oncology Department IV of Beijing Tiantan Hospital (BTH) between January 2019 and December 2021. Inclusion criteria were as follows: (a) Availability of comprehensive tumor histopathological and molecular profiling data; (b) Confirmation of tissue-based diagnosis according to the WHO 2021 classification criteria for either A4 or Glioblastoma, IDH-wild-type, WHO Grade 4; and (c) Accessibility to clinical treatment records, including a minimum follow-up period of ≥ 3 months post-surgery to ascertain histopathological diagnosis. The process of patient enrollment was meticulously delineated in a flowchart (Figure S1). Additionally, 401 eligible patients from the UCSF Preoperative Diffuse Glioma MRI Dataset (PDGM) were included as an external validation cohort.

2.2 Histopathologic review and molecularly integrated diagnosis

Histopathological assessment of all tumors was conducted at the Department of Neuropathology of BTH by a panel of three senior neuropathologists (G.H.D., Z.F.G., and D.H.L.), each possessing over 20 years of experience in the field. These neuropathologists were blinded to patients' clinical, radiological, and outcome data. Subsequently, an integrated diagnosis was formulated by meticulously reviewing both the histopathological characteristics and molecular biomarkers, which included assessments of chromosome 1p/19q, IDH1/2, TERT, EGFR, CDKN2A/B, and the status of chromosomes 7 and 10. All gliomas were categorized as either A4 or Glioblastoma in accordance with the 2021 WHO CNS 5 classification. In instances of discordance, a final diagnosis was established through consensus. Chromosome 1p and 19q analysis was performed by fluorescence in situ hybridization (FISH). IDH status was determined via DNA sequencing, and O6-methylguanine-DNA methyltransferase (MGMT) promoter methylation was assessed by pyrosequencing bisulfite-treated genomic DNA. Details on the experimental protocols and interpretation principles have been elaborated on in our previous studies. Additional information regarding the methodologies employed for immunohistochemistry, sequencing techniques, FISH, and pyrosequencing can be referenced in prior publications [19–23].

2.3 Neuroimaging assessment

A comprehensive neuroimaging assessment was conducted by a multidisciplinary team comprising two senior neuroradiologists (H.Y.C. and X.Z.C.) and one experienced neurosurgeon (X.H.R.), each possessing over 15 years of experience in neuroimaging. Radiological evaluations encompassed an array of features, including tumor localization, tumor size (both contrast-enhancing (CE) tumor, and non-CE tumor), involvement of the subventricular zone (SVZ), extent of resection (EOR), cortical non-enhancing tumor infiltration (CnCE), margin clarity, and the presence of enhancement, necrosis, cysts, calcification, and hemorrhage. Discriminative radiological features were extracted based on the Visually Accessible Rembrandt Images (VASARI: https://wiki.nci.nih.gov/display/CIP/VASARI) feature set. Total CE tumor was measured utilizing contrast-enhanced T1-weighted sequences, while non-CE tumor was evaluated on FLAIR/T2-weighted sequences. Identification of non-CE tumor relied on disruptions in anatomical architecture and the FLAIR/T2 signal intensity relative to cerebrospinal fluid or normal white matter. Patients were classified as having non-CE tumor when preoperative imaging revealed ≤ 1 cm^3 of contrast enhancement, with no discernible difference demonstrated between individuals exhibiting minimal CE (0–1 cm^3) and those lacking contrast enhancement, after accounting for non-CE tumor [24–26].

Tumor dimensions were quantified using the maximal Feret diameter, representing the longest achievable distance in any direction within a non-symmetric area, and the ratio of CE tumor diameter to non-CE tumor diameter (CE/nCE) was calculated accordingly. Multifocal disease was assessed separately for each focus and subsequently aggregated. CnCE was defined as an area of FLAIR hyperintensity confined to the cortical grey matter, devoid of contrast enhancement and with or without involvement of the underlying white matter (Figure S2). Tumors infiltrating the walls of the lateral ventricles were categorized as SVZ-involved, with further subclassification into Type I-IV [27]. EOR was determined based on the volume of resected tumor observed on 48–72-h postoperative MR images and classified as gross-total resection (GTR, ≥ 99%), near-total resection (NTR, 95–99%), and subtotal resection (STR, < 95%).

2.4 Treatment protocol

All patients underwent tumor resection at our institution, followed by subsequent interventions involving radiotherapy and chemotherapy as warranted. Radiotherapy was administered at a total dose ranging from 54 to 60 Gy, either as standalone treatment or in conjunction with temozolomide-based concomitant chemotherapy (75 mg/m^2/day). Adjuvant chemotherapy regimens adhered to classic Stupp protocols. A minimum of 6 cycles of adjuvant chemotherapy was prescribed, provided the patient demonstrated tolerability to the regimen.

2.5 Follow-up

Patients were followed until death or date of database closure (April 1, 2023). Patients who were still alive or lost to follow-up at the time of statistical analysis were considered as censored events. The assessment of treatment response was based on RANO criteria [28]. Overall survival (OS) was calculated as the duration from the date of diagnosis to death from any cause. At the time of database closure, 70 patients were alive (31.4%), including 11 patients lost to follow-up (not seen for ≥ 12 months), and 153 patients were deceased (68.6%).

2.6 Predictive model construction and evaluation

In the BTH cohort (the training set), we conducted a "least absolute shrinkage and selection operator (LASSO) regression" analysis to screen predictor variables. After identifying the relevant predictors for the A4 subtype in Grade 4 gliomas, we constructed the predictive model using the "lrm" function in the Design package in RStudio. The model was visualized using the "nomogram" function in the "regplot" package. The optimal cutoff value was determined by calculating the maximal Youden index through receiver operating characteristic (ROC) curve analysis, which also provided the area under the curve (AUC) for both the training and validation sets. To further evaluate the model in the external validation set, we employed a calibration curve and Decision Curve Analysis (DCA).

2.7 Statistical analysis

Patient demographics and tumor characteristics were summarized with descriptive statistics. Categorical comparisons among different groups were conducted using the chi-square test or Fisher's exact test, as appropriate. Differences in age distribution, MGMT promoter methylation levels, and tumor size were assessed using unpaired Student's t-test, while differences among multiple groups were analyzed using one-way ANOVA. For nonparametric data, the Mann–Whitney U-test was employed for comparisons between two groups, and the Kruskal–Wallis test was used for comparisons among multiple groups. Survival analysis was conducted using the Kaplan–Meier method for univariate analysis, and differences between survival curves were compared using the log-rank test. For multivariate survival analysis, Cox proportional hazard regression models were constructed to estimate hazard ratios (HR) and corresponding 95% confidence intervals (CI). All statistical analyses were performed using SPSS (version 22.0) and R software (http://www.r-project.org). Two-sided tests were used for all analyses, with statistical significance defined as $p < 0.05$.

3 Results

3.1 Patient cohorts

A total of 223 patients diagnosed with either glioblastomas or A4 were included in this study, comprising 138 males and 85 females, with a median age of 55 years (range, 6–77) at the time of initial diagnosis. All tumors were classified as WHO Grade 4 according to the WHO 2021 classification. Pathological examination revealed that 201 patients (90.1%) had glioblastomas, while 22 patients (9.9%) had A4. The diagnosis was based on the presence of histopathological features consistent with glioblastomas, accompanied by IDH-wildtype status (referred to as histologic glioblastoma, hGBM), observed in 183 patients (82.1%). In cases lacking classical histopathological features of glioblastomas, the diagnosis was established through the combination of IDH-wildtype status with other qualifying molecular markers (such as TERT promoter mutations, EGFR amplifications, or chromosomes + 7/− 10 genotype, termed molecular glioblastoma, mGBM), involving the remaining 18 patients (8.1%). A comprehensive summary of the clinical, radiological, and molecular characteristics of the cohort is provided in Fig. 1. An overview of patients' basic characteristics in UCSF PDGM set was provided in Table S1.

3.2 Comparison of basic characteristics between mGBM and hGBM

Age and gender distributions exhibited no significant differences between the mGBM and hGBM groups ($p > 0.05$). Notably, patients with mGBM demonstrated a relatively lower incidence of preoperative neurologic deficits (11.1% vs. 34.4%, $p = 0.079$), but a higher prevalence of epilepsy (55.6% vs. 23.0%, $p = 0.008$), compared to those with hGBM. Anatomically, tumors in both groups were predominantly located superficially ($p > 0.05$). However, mGBM patients presented with smaller tumor sizes, including CE tumor and non-CE tumor, and exhibited a reduced extent of partial CE lesions compared to hGBM patients ($p < 0.001$). Notably, about 77.8% mGBM patients exhibited none to minimal CE on preoperative imaging, compared to 4.0% in the hGBM group ($p < 0.001$). Additional radiological observations revealed that mGBM patients displayed a lower prevalence of SVZ involvement, necrosis, and smooth margins while manifesting a higher incidence of CnCE and involvement of insular lobes compared to hGBM patients ($p < 0.05$). Regarding molecular characteristics, all mGBM patients harbored TERT promoter mutations, predominantly of TERT C228T subtype ($n = 13$, 72.2%), whereas in the hGBM group, TERT promoter mutations were distributed as follows: TERT C228T in 90 patients (49.5%), TERT C250T in 28 patients (15.4%), and wild-type in 64 patients (35.2%). However, there were no significant differences between the two groups in terms of MGMT promoter methylation levels and EGFR amplifications ($p > 0.05$). With respect to treatment modalities, no significant disparities were observed between the two groups concerning EOR, postoperative radiotherapy coverage, or the incidence of secondary surgeries ($p > 0.05$). Notably, mGBM patients underwent significantly fewer postoperative chemotherapy sessions compared to hGBM patients (83.3% vs. 96.4%, $p = 0.045$) (Table 1).

3.3 Comparison of basic characteristics between A4 and hGBM

Our investigation revealed that patients diagnosed with A4 tended to be younger than those with hGBM (39.8 ± 11.5 vs. 53.8 ± 12.7, $p < 0.001$), while exhibiting comparable gender distributions and clinical symptomatology ($p > 0.05$). Notably, the incidence of CnCE was significantly higher among A4 patients compared to hGBM patients (81.8% vs. 20.6%, $p < 0.001$). Relative to the hGBM cohort, the A4 group displayed smaller CE tumor, lower enhancement ratios, higher frequencies of cystic changes, and clearer boundaries (CE tumor: 30.0 ± 22.4 vs. 41.6 ± 16.0, $p = 0.032$; CE ratio: 59.1% vs. 96.0%, $p < 0.001$; Cyst: 40.9% vs. 19.7%, $p = 0.031$; Smooth margin: 72.7% vs. 44.4%, $p = 0.022$). Furthermore, A4 lesions were more prone to cortical and SVZ involvement ($p = 0.024$), while rates of necrosis, calcification, and hemorrhage were comparable between the two groups ($p > 0.05$). Additionally, there were no significant disparities observed in treatment modalities between the two cohorts. Regarding molecular characteristics, A4 patients demonstrated a higher level of MGMT methylation (29.0 ± 19.8% vs. 17.1 ± 19.9%, $p < 0.001$), and a lower rate of TERT promoter mutation (18.1% vs. 64.9%, $p < 0.001$) (Table 1).

3.4 Prognostic implications of distinct WHO Grade 4 gliomas

There was no discernible difference in OS between patients with mGBM and those with hGBM (21.2 vs. 20.0 months, $p = 0.454$) (Fig. 2A). It is noteworthy that patients with mGBM were less frequently administered postoperative radiochemotherapy compared to those with hGBM (77.8% vs. 94.0%, $p = 0.045$) (Fig. 2B). However, no significant disparity was

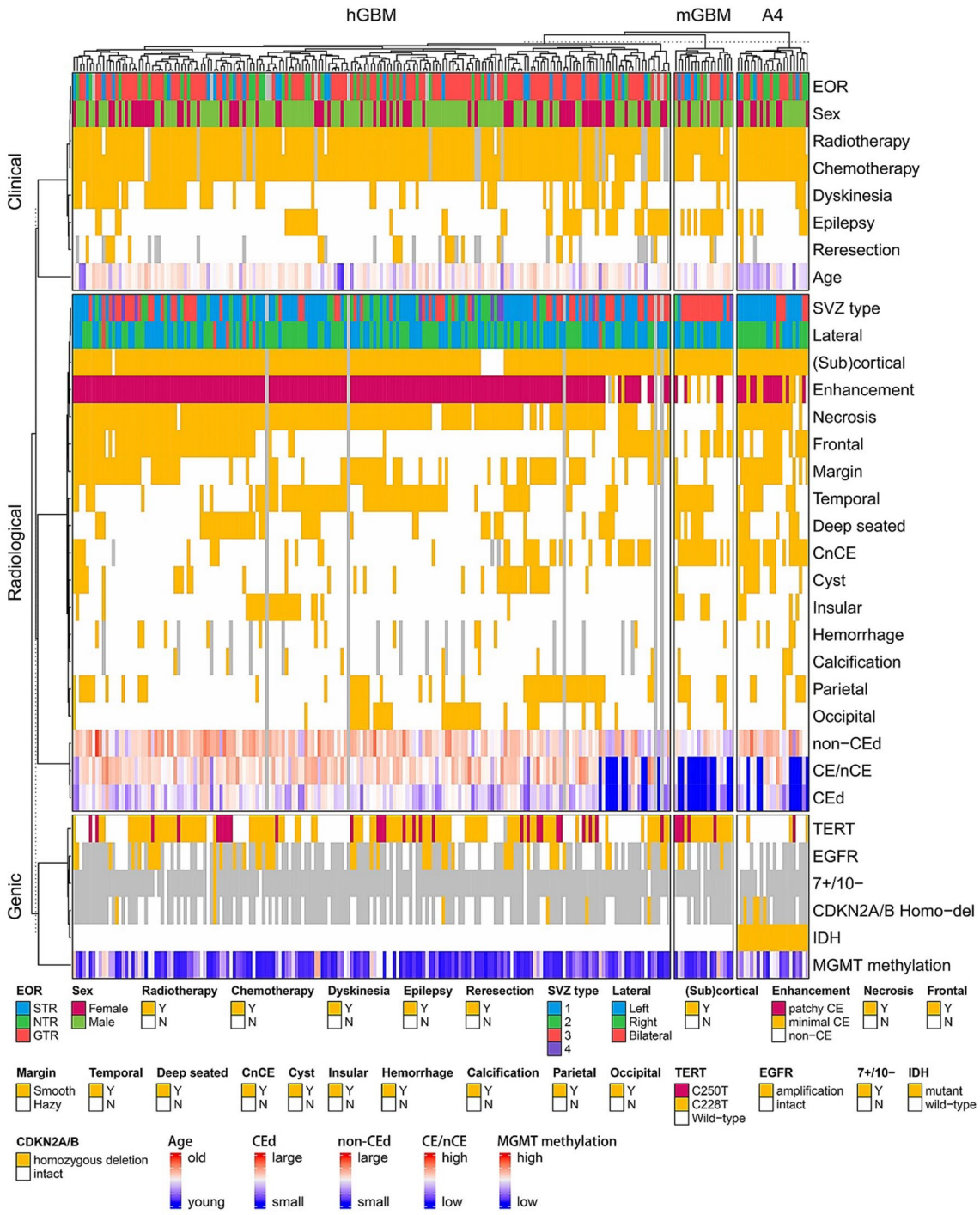

Fig. 1 Heatmap including basic characteristics for Grade 4 gliomas. Histologic glioblastoma tends to manifest with advanced age and high enhancement rates, along with low MGMT methylation levels. And the cortical non-enhancing tumor infiltration sign was more common in A4, while low enhancement rates and absence of necrosis were more specific for molecular glioblastoma. *A4* Astrocytoma, IDH-mutant, WHO Grade 4

observed between mGBM and hGBM when the comparison focused on patients receiving postoperative radiochemotherapy (21.2 vs. 20.6 months, $p = 0.906$) (Fig. 2C). In contrast, patients with A4 demonstrated superior survival compared to those with hGBM ($p < 0.001$) or mGBM ($p = 0.005$) (Fig. 2A). And the median follow-up durations were 41.6 months for hGBM patients, 38.4 months for mGBM patients, and 46.9 months for A4 patients ($p > 0.05$). These findings were consistent in the UCSF PDGM cohort (Figure S3). In the following multivariate analysis, the prognostic significance of A4

Table 1 Comparison of basic characteristics among Grade 4 gliomas

	IDH-wt hGBM (n = 183)	IDH-wt mGBM (n = 18)	IDH-mut A4 (n = 22)	P (mGBM vs. hGBM)	P (A4 vs. hGBM)
Sex, male (%)	112 (61.2)	13 (72.2)	13 (59.1)	0.506	> 0.999
Age (years, mean ± SD)	53.8 ± 12.7	54.1 ± 8.7	39.8 ± 11.5	0.634	< 0.001
MGMT (%, mean ± SD)	17.1 ± 19.9	16.5 ± 20.2	29.0 ± 19.8	0.649	< 0.001
TERT (%)				0.002	< 0.001
Wild-type	64 (35.2)	0 (0.0)	18 (81.8)		
C228T	90 (49.5)	13 (72.2)	3 (13.6)		
C250T	28 (15.4)	5 (27.8)	1 (4.5)		
WHO grade (%)				< 0.001	< 0.001
2	0 (0.0)	10 (55.6)	2 (9.1)		
3	0 (0.0)	8 (44.4)	4 (18.2)		
4	183 (100)	0 (0.0)	16 (72.7)		
Epilepsy (%)	42 (23.0)	10 (55.6)	8 (36.4)	0.008	0.262
Dyskinesia (%)	63 (34.4)	2 (11.1)	3 (13.6)	0.079	0.084
EOR (%)				0.406	0.099
STR	28 (16.2)	5 (29.4)	3 (13.6)		
NTR	34 (19.7)	3 (17.6)	9 (40.9)		
GTR	111 (64.2)	9 (52.9)	10 (45.5)		
Chemotherapy (%)	161 (96.4)	15 (83.3)	22 (100.0)	0.045	> 0.999
Radiotherapy (%)	161 (96.4)	16 (88.9)	21 (95.5)	0.176	0.586
Lateral (%)				0.100	0.085
Left	92 (50.8)	14 (77.8)	6 (27.3)		
Right	83 (45.9)	4 (22.2)	15 (68.2)		
Bilateral	6 (3.3)	0 (0.0)	1 (4.5)		
SVZ (%)				0.001	0.024
Type I	82 (46.1)	2 (11.1)	17 (77.3)		
Type II	31 (17.4)	1 (5.6)	0 (0.0)		
Type III	56 (31.5)	14 (77.8)	5 (22.7)		
Type IV	9 (5.1)	1 (5.6)	0 (0.0)		
CE tumor diameter (mm, mean ± SD)	41.6 ± 16.0	12.0 ± 14.8	30.0 ± 22.4	< 0.001	0.032
Non-CE tumor diameter (mm, mean ± SD)	67.3 ± 19.1	50.2 ± 13.6	69.4 ± 20.1	< 0.001	0.59
CE/nCE (mean ± SD)	0.60 ± 0.22	0.15 ± 0.25	0.36 ± 0.30	< 0.001	< 0.001
Deep-seated (%)	44 (24.7)	7 (38.9)	8 (36.4)	0.257	0.359
(Sub-)cortical (%)	170 (95.5)	18 (100.0)	22 (100.0)	> 0.999	0.602
Frontal (%)	74 (41.6)	9 (50.0)	14 (63.6)	0.660	0.082
Temporal (%)	76 (42.7)	12 (66.7)	10 (45.5)	0.089	0.985

Discover Oncology (2025) 16:111 | https://doi.org/10.1007/s12672-025-01811-0

Table 1 (continued)

	IDH-wt hGBM (n = 183)	IDH-wt mGBM (n = 18)	IDH-mut A4 (n = 22)	P (mGBM vs. hGBM)	P (A4 vs. hGBM)
Parietal (%)	50 (28.1)	7 (38.9)	6 (27.3)	0.491	> 0.999
Occipital (%)	35 (19.7)	2 (11.1)	1 (4.5)	0.534	0.136
Insular (%)	22 (12.4)	6 (33.3)	5 (22.7)	0.027	0.189
Enhancement (%)				< 0.001	< 0.001
Non-CE	5 (2.8)	11 (61.1)	2 (9.1)		
Minimal CE	2 (1.1)	3 (16.7)	7 (31.8)		
Predominant CE	170 (96.0)	4 (22.2)	13 (59.1)		
Necrosis (%)	158 (88.8)	2 (11.1)	18 (81.8)	< 0.001	0.311
Cyst (%)	35 (19.7)	1 (5.6)	9 (40.9)	0.205	0.031
Smooth margin (%)	79 (44.4)	2 (11.1)	16 (72.7)	0.013	0.022
CnCE (%)	36 (20.6)	14 (77.8)	18 (81.8)	< 0.001	< 0.001
Calcification (%)	8 (4.9)	1 (5.6)	3 (13.6)	> 0.999	0.128
Hemorrhage (%)	13 (8.0)	1 (5.6)	4 (18.2)	> 0.999	0.125
Re-resection (%)	19 (11.8)	1 (5.9)	1 (4.8)	0.697	0.477

hGBM histologic glioblastoma, *mGBM* molecular glioblastoma, *A4* Astrocytoma, IDH-mutant, WHO grade 4, *IDH-wt* isocitrate dehydrogenase wild-type, *MGMT* O6-methylguanine-DNA methyltransferase, *TERT* telomerase reverse transcriptase, *EOR* extent of resection, *STR* subtotal resection, NTR near-total resection, *GTR* gross-total resection, *SVZ* subventricular zone, *CE* contrast-enhancing, *CE/nCE* CE tumor diameter/ non-CE tumor diameter, *CnCE* cortical non-CE tumor infiltration

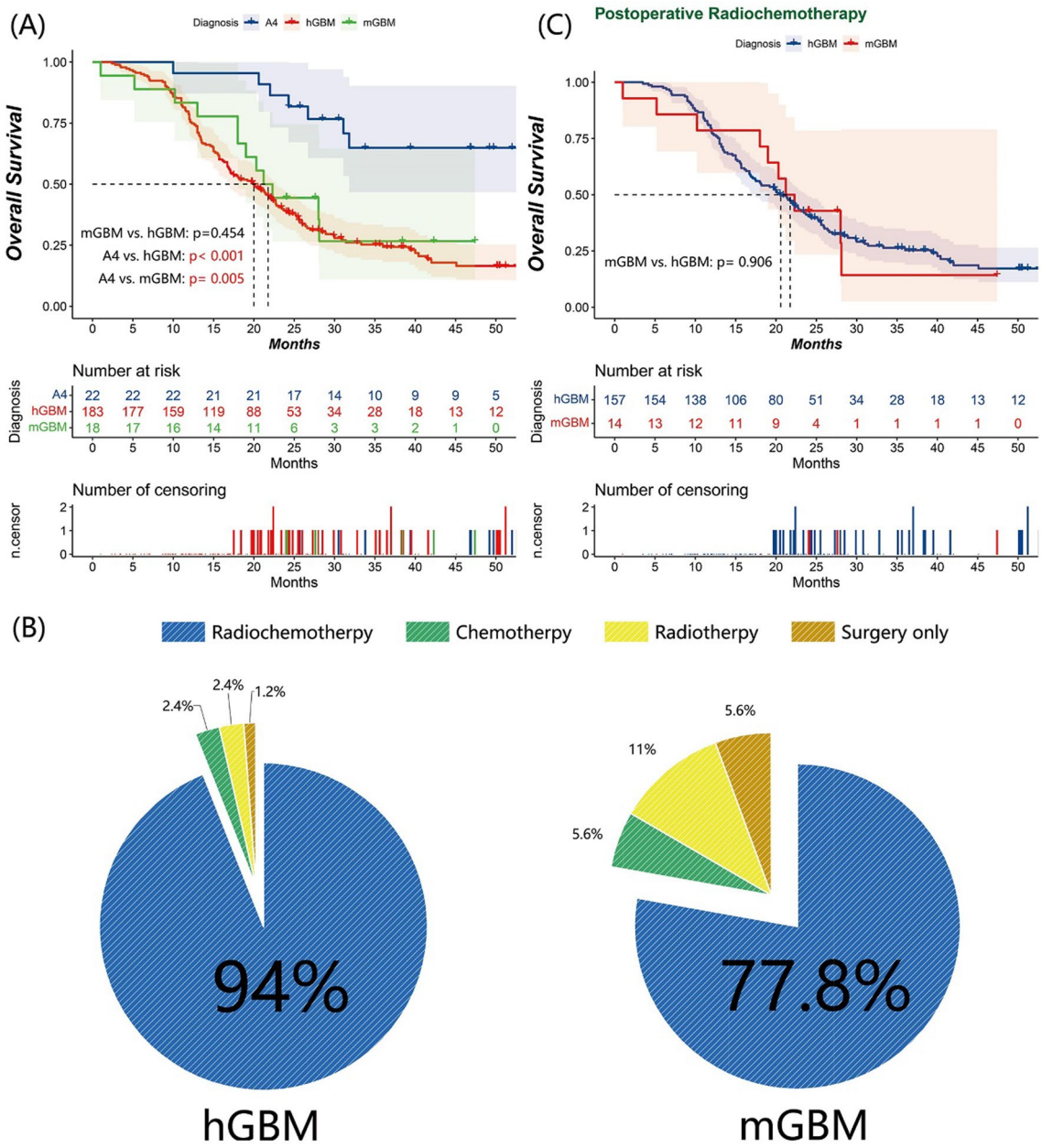

Fig. 2 **A** prognostic implications of different Grade 4 glioma in overall survival. **B** distribution of therapeutic approaches following resection between histologic glioblastoma and molecular glioblastoma. **C** survival comparison between molecular glioblastoma and histologic glioblastoma in patients received postoperative radiochemotherapy

was still upheld (HR: 0.39, CI 0.17–0.91; p = 0.03) (Table 2). Furthermore, GTR (HR: 0.35, CI 0.22–0.56; p < 0.001), NTR (HR: 0.57, CI 0.33–0.99; p = 0.044), higher MGMT methylation level (HR: 0.98, CI 0.97–0.99; p < 0.001), and CnCE (HR: 0.54, CI 0.35–0.83; p = 0.005) were confirmed as independent prognostic factors associated with favorable survival, while tumor deep localization (HR: 1.96, CI 1.33–2.88; p = 0.001) was independent prognostic risk factor.

3.5 Integrated model for predicting A4

Given the significant clinical implications associated with A4, there is an urgent need for predictive models to identify this subtype. The LASSO path diagram (Fig. 3A) illustrates how the number of predictors decreases as the coefficients shrink. In the LASSO selection path diagram (Fig. 3B), two specific λ values, lambda.min and lambda.1se,

Table 2 Univariate and multivariate survival analyses based on all patients with grade 4 glioma

Characteristic	N	Univariate analysis		Multivariate analysis	
		Hazard ratio (95% CI)	p	Hazard ratio (95% CI)	p
Age (years)	223	1.020 [1.007, 1.034]	0.003	1.013 [0.998, 1.028]	0.091
MGMT methylation level (%)	223	0.986 [0.977, 0.995]	0.002	0.982 [0.973, 0.992]	< 0.001
CE tumor diameter (mm)	218	1.005 [0.997, 1.013]	0.217		
Non-CE tumor diameter (mm)	218	1.006 [0.998, 1.014]	0.153		
CE/nCE (%)	218	1.245 [0.680, 2.279]	0.477		
Sex (Female vs. Male)	138	1.016 [0.732, 1.408]	0.926		
TERT (reference wild-type)					
C228T	106	1.593 [1.108, 2.292]	0.012	1.230 [0.817, 1.852]	0.322
C250T	34	1.609 [1.003, 2.580]	0.048	1.041 [0.617, 1.755]	0.881
WHO grade (reference 2)					
3	12	1.449 [0.515, 4.073]	0.482		
4	199	1.641 [0.724, 3.719]	0.235		
mGBM	18	0.926 [0.514, 1.671]	0.8		
A4	22	0.239 [0.111, 0.511]	< 0.001	0.389 [0.165, 0.914]	0.03
Epilepsy	60	0.840 [0.582, 1.213]	0.354		
Dyskinesia	68	1.150 [0.817, 1.619]	0.423		
EOR (reference STR)					
NTR	46	0.522 [0.318, 0.858]	0.01	0.571 [0.331, 0.986]	0.044
GTR	130	0.414 [0.273, 0.626]	< 0.001	0.348 [0.217, 0.559]	< 0.001
Chemotherapy	198	0.992 [0.406, 2.423]	0.986		
Radiotherapy	198	0.814 [0.359, 1.846]	0.622		
SVZ involvement	133	1.084 [0.778, 1.511]	0.633		
Deep-seated	59	1.789 [1.266, 2.529]	0.001	1.958 [1.329, 2.884]	0.001
(Sub-)cortical	210	0.664 [0.293, 1.505]	0.327		
Enhancement (reference non-CE)					
Minimal CE	12	0.574 [0.212, 1.559]	0.276		
Predominant CE	187	1.168 [0.631, 2.162]	0.622		
Necrosis	178	1.069 [0.695, 1.642]	0.762		
Cyst	45	0.646 [0.425, 0.981]	0.04	0.791 [0.501, 1.251]	0.317
Smooth margin	97	0.700 [0.506, 0.969]	0.032	0.999 [0.691, 1.446]	0.997
CnCE	68	0.578 [0.399, 0.837]	0.004	0.538 [0.349, 0.828]	0.005
Calcification	12	0.719 [0.334, 1.547]	0.399		
Hemorrhage	18	1.460 [0.823, 2.590]	0.195		
Re-resection	21	0.736 [0.423, 1.280]	0.277		

MGMT O6-methylguanine-DNA methyltransferase, *CE* contrast-enhancing, *CE/nCE* CE tumor diameter/non-CE tumor diameter, *TERT* telomerase reverse transcriptase, *mGBM* molecular glioblastoma, *A4* Astrocytoma, IDH-mutant, WHO grade 4, *EOR* extent of resection, *STR* subtotal resection, *NTR* near-total resection, *GTR* gross-total resection, *SVZ* subventricular zone, *CnCE* cortical non-CE tumor infiltration

are highlighted. Based on lambda.1se, we selected three variables from Table 1—CnCE sign, age at diagnosis, and tumor margin—to construct the model. After determining the final variables for the A4 prediction model in Grade 4 glioma patients, we constructed the model in RStudio using the lrm function in the "rms" package and generated a nomogram using the "regplot" package (Fig. 3C, C-index: 0.890). The area under the ROC curve (AUC) for the A4 prediction model was 0.890 (95% CI 0.816–0.963) in the training set and 0.951 (95% CI 0.916–0.985) in the validation set (Fig. 3D). In the validation set, the Brier score for the calibration curve was 0.035 (Fig. 3E). The DCA curves indicated that the predictive model developed in this study offers a significant net benefit (Fig. 3F).

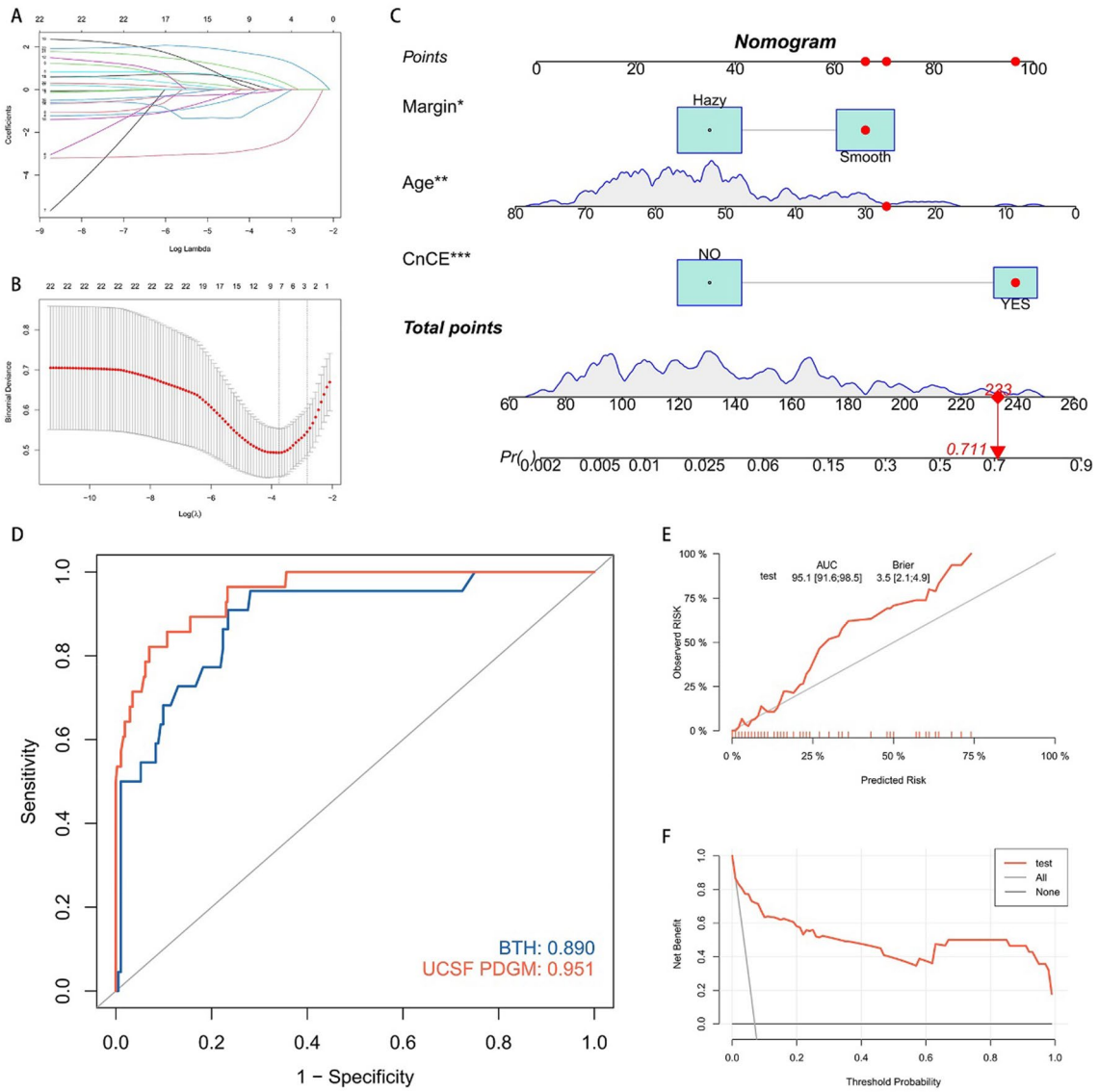

Fig. 3 **A** LASSO Path Plot: This plot illustrates the regression coefficients versus Log(λ) as the coefficient scores gradually decrease. The coefficients correspond to each independent variable in the model. **B** LASSO Selection Path Plot: Vertical dashed lines on the left side of the plot represent Log(λ) corresponding to the minimum error (lambda.min), while the vertical dashed lines on the right side represent Log(λ) that is one standard error away from the minimum error (lambda.1se). The Binomial Deviance represents the binomial distribution loss function of the model, computed on each fold during the cross-validation process. **C** Nomogram: This visual tool sums the scores from each predictor (e.g., younger age earned the highest score, and the presence of CnCE as well as smooth margin are positively correlated with the likelihood of A4). The total score predicts the probability of A4 occurring. **D** ROC Analysis of the Model: the model achieved an AUC of 0.890 in the BTH cohort (training set). In the UCSF PDGM cohort (validation set), the AUC improved to 0.951, indicating excellent model performance. **E** Calibration Curves: The curves indicate a reasonable agreement between the predicted probability of A4 and its actual occurrence (Brier score: 0.035). **F** Decision Curve Analysis (DCA): This chart demonstrates that the model provides a higher net benefit compared to the "treat-all" and "treat-none" strategies, highlighting its potential clinical utility. The x-axis represents the threshold probability, which is the probability of A4 at which a clinician might choose to intervene. The y-axis represents the net benefit, calculated by incorporating true positive and false positive predictions into a single metric

4 Discussion

Under the 2021 WHO classification, Grade 4 gliomas represent a diverse cohort, displaying a spectrum of clinical, radiological, and molecular characteristics. This updated classification has sparked considerable discourse within the research community [12, 13]. In this study, we aimed to delve into the clinicoradiological, molecular, and therapeutic

dimensions of WHO Grade 4 gliomas.

In our cohort, mGBM exhibited clinical and neuroradiological profiles largely resembling those of IDH-mutant astrocytomas. Predominantly, these tumors manifested in the frontal and temporal lobes and were often associated with seizures as the initial clinical presentation. The frequency of seizures of patient with mGBM at presentation (55.6%) was slightly lower compared to those with IDH-mutant Grade 2 astrocytomas (70–80%) [29]. Besides, about 38.9% of mGBM patients exhibited mild or patchy contrast enhancement on MRI, consistent with findings reported elsewhere [30]. Moreover, none of non-CE tumor displayed evidence of necrosis (0/14) in mGBM cohort, which corroborated the findings from prior investigations [31]. In the mGBM subgroup, patients exhibited similar ages to those with hGBM, yet tended to present with smaller tumor volumes on MRI. Additionally, a significant proportion of mGBM tumors (over three-quarters) demonstrated cortical involvement, aligning with previous research [32].

Conversely, mGBM displayed molecular features and prognostic outcomes akin to hGBM. In this study, TERT mutations were prevalent in mGBM, consistent with prior literature [10]. Alongside the molecular hallmarks of glioblastomas, the MGMT methylation level of mGBM mirrored that of hGBM. Even upon multivariate analysis, MGMT methylation persisted as a prognostic indicator, corroborating numerous earlier reports [24–26]. The relatively low methylation level observed in mGBM may contribute to its unfavorable prognosis. However, in contrast to earlier studies [8], the prognostic relevance of the TERT phenotype diminished in multivariate analysis. Notably, our study revealed no significant disparities in survival outcome between mGBM and hGBM. The median survival of mGBM was 21.2 months, which aligned with the reported range of 20.8–31.9 months in previous research [8–11]. Moreover, in our series mGBM patients with isolated TERT promoter mutations have a significantly worse OS (19 months) as compared to the results reported by Berzero et al. [12] (88 months). It reinforces the argument for reclassifying the subtype of IDH wild-type astrocytoma as WHO Grade 4. However, our study did not identify a prognostic advantage for histological Grade 2 mGBM compared to Grade 3, contrary to earlier investigations [10, 11, 13].

Our investigation unveiled a notably favorable prognosis for A4 compared to hGBM, marked by a median survival that remained undefined and a median follow-up duration extending to 46.9 months, surpassing previous literature findings [4–6, 14–17, 33]. The high rate of resection and comprehensive radiochemotherapy coverage observed in our study may contribute to this enhanced prognosis. Additionally, distinct features of A4, including younger age, elevated MGMT methylation levels, reduced incidence of TERT mutations, and limited enhancement, likely contribute to its favorable prognosis. Moreover, even upon rigorous multivariate analysis, the prognostic advantage of A4 persisted significantly, which underscored the prognostic implication of IDH mutation.

Furthermore, it appears that many characteristics of low-grade gliomas can also be identified in A4. In terms of radiological characteristics, our investigation underscores that the predominant majority of A4 cases (82%) present CnCE feature, which has been labelled as "low-grade appearance", consistent with earlier research [31, 34–36]. Hence, we included the CnCE in our integrated model to predict A4 phenotype. Similarly, Lasocki et al. [35] found a close relationship between mass-like non-CE tumor morphology in GBM and the IDH mutation phenotype. Additionally, our findings reveal partial enhancement in A4, primarily due to the prevalence of enhancing characteristics in A4 tumors alongside a relatively large proportion of non-CE tumor [34, 37], consistent with prior research findings [31]. From a hispathological perspective, Qiu et al. [33] found that over 50% of A4 histopathologies exhibit components of low-grade gliomas, a proportion significantly higher than that observed in IDH wild-type glioblastoma. In terms of molecular characteristics, previous studies have identified genetic similarities between de novo primary A4 and evolved secondary A4 (initially diagnosed as Grade 2 or Grade 3 astrocytomas [38, 39], suggesting a potential secondary transformation of A4 from low-grade gliomas [7]. All these low-grade gliomas characteristics may contribute to the relatively favorable clinical outcome of A4.

Moreover, our study elucidates that patient with CnCE shows a more favorable prognosis. This protective prognostic attribute even persists after multivariable analysis. In line with previous investigations, primary A4 patients presenting with mixed low-grade gliomas components also demonstrate enhanced clinical outcomes [33]. Both preoperative imaging and histopathological assessments suggest a more favorable prognosis for A4 tumors exhibiting characteristics consistent with low-grade gliomas. This observation may imply an early morphological transition of A4 from a low-grade glioma to a secondary glioblastoma. Although prior studies did not confirm the prognostic advantage of mixed pathology in secondary A4 [33], it is important to acknowledge that these studies primarily assessed survival periods from the confirmation of Grade 4 glioma through a second surgery to the occurrence of events, without considering the disease course of initially diagnosed Grade 2 or Grade 3 astrocytoma.

This study is subject to several limitations. Firstly, its retrospective design introduces inherent biases related to patient selection. Secondly, the relatively low incidence of primary A4 and mGBM limits the depth of consecutive patient enrollment in this single-center study. Thirdly, the predictive models developed for A4 do not encompass Grade 3 gliomas and

low-grade gliomas, potentially limiting their clinical applicability to some extent. Lastly, ongoing follow-up until the last patient reaches the endpoint is necessary to validate the results and conclusions drawn from this research.

In conclusion, our study sheds light on the complex landscape of Grade 4 gliomas, particularly A4 and mGBM, under the updated WHO classification. Through comprehensive analysis encompassing clinical, radiological, molecular, and therapeutic aspects, we have uncovered distinct characteristics and prognostic implications associated with these glioma subtypes. Our findings underscore the importance of integrating multimodal approaches, including neuroimaging features and molecular profiling, to accurately diagnose and prognosticate Grade 4 gliomas. Moreover, the development of predictive models for A4 holds promise for enhancing preoperative assessment and guiding personalized treatment strategies.

Acknowledgements The authors would like to thank Gehong Dong, Zhifen Gao and Dehong Lu, Department of Pathology, Beijing Tiantan Hospital, Capital Medical University, for pathology diagnosis, and Hongyan Chen, Xuzhu Chen, Department of Neuroradiology, Beijing Tiantan Hospital, Capital Medical University, for radiological evaluation. We also appreciate all patients and their families for cooperation during follow-up.

Author contributions Acquisition of data: H.J.,X.W., S.Z., and X.R.; Analysis and Interpretation of Data: H.J.,X.W., Q.R., and Y.C.; Statistical analysis: H.J.,X.W., M.L, M.L., and Y.C.; Drafting the Article: H.J.,X.W., and X.C.; Critically Revising the Article: H.J.,X.W., X.C., Y.C. and S.L.; funding acquisition: H.J.; Conception and Design: H.J., Y.C., and S.L.; and study supervision: Y.C. and S.L.

Funding This research was supported by the National Natural Science Foundation of China (No.82202983) and Peking University Clinical Scientist Training Program, supported by "the Fundamental Research Funds for the Central Universities".

Data availability The original contributions presented in this study are included in the article/Supplementary Material. Further inquiries can be directed to the corresponding authors.

Declarations

Ethics approval and consent to participate Approval of the research protocol by an Institutional Reviewer Board: This study conformed to the ethical guidelines of the 1975 Declaration of Helsinki and was approved by the Institutional Review Board of Beijing Tiantan Hospital (BTH).

Informed consent Given the retrospective design, the BTH Institutional Review Board approved the performance of this study with a waiver of informed consent.

Competing interests The authors declare no competing interests.

References

1. Louis DN, et al. The 2021 WHO classification of tumors of the central nervous system: a summary. Neuro Oncol. 2021;23(8):1231–51. https://doi.org/10.1093/neuonc/noab106.
2. Brat DJ, et al. cIMPACT-NOW update 3: recommended diagnostic criteria for "Diffuse astrocytic glioma, IDH-wildtype, with molecular features of glioblastoma, WHO grade IV." Acta Neuropathol. 2018;136(5):805–10. https://doi.org/10.1007/s00401-018-1913-0.
3. Brat DJ, et al. cIMPACT-NOW update 5: recommended grading criteria and terminologies for IDH-mutant astrocytomas. Acta Neuropathol. 2020;139(3):603–8. https://doi.org/10.1007/s00401-020-02127-9.
4. Eckel-Passow JE, et al. Glioma groups based on 1p/19q, IDH, and TERT promoter mutations in tumors. N Engl J Med. 2015;372(26):2499–508. https://doi.org/10.1056/NEJMoa1407279.
5. Brat DJ, et al. Comprehensive, integrative genomic analysis of diffuse lower-grade gliomas. N Engl J Med. 2015;372(26):2481–98. https://doi.org/10.1056/NEJMoa1402121.
6. Cimino PJ, et al. Multidimensional scaling of diffuse gliomas: application to the 2016 world health organization classification system with prognostically relevant molecular subtype discovery. Acta Neuropathol Commun. 2017;5(1):39. https://doi.org/10.1186/s40478-017-0443-7.
7. Hata N, et al. Insular primary glioblastomas with IDH mutations: clinical and biological specificities. Neuropathology. 2017;37(3):200–6. https://doi.org/10.1111/neup.12362.
8. Rudà R, et al. IDH wild-type grade 2 diffuse astrocytomas: prognostic factors and impact of treatments within molecular subgroups. Neuro Oncol. 2022;24(5):809–20. https://doi.org/10.1093/neuonc/noab239.

9. Tesileanu CMS, et al. Survival of diffuse astrocytic glioma, IDH1/2 wildtype, with molecular features of glioblastoma, WHO grade IV: a confirmation of the cIMPACT-NOW criteria. Neuro Oncol. 2020;22(4):515–23. https://doi.org/10.1093/neuonc/noz200.
10. Nakasu S, Deguchi S, Nakasu Y. IDH wild-type lower-grade gliomas with glioblastoma molecular features: a systematic review and meta-analysis. Brain Tumor Pathol. 2023;40(3):143–57. https://doi.org/10.1007/s10014-023-00463-8.
11. Makino Y, et al. Prognostic stratification for IDH-wild-type lower-grade astrocytoma by sanger sequencing and copy-number alteration analysis with MLPA. Sci Rep. 2021;11(1):14408. https://doi.org/10.1038/s41598-021-93937-8.
12. Berzero G, et al. IDH-wildtype lower-grade diffuse gliomas: the importance of histological grade and molecular assessment for prognostic stratification. Neuro Oncol. 2021;23(6):955–66. https://doi.org/10.1093/neuonc/noaa258.
13. Giannini C, Giangaspero F. TERT promoter mutation: is it enough to call a WHO grade II astrocytoma IDH wild-type glioblastoma? Neuro Oncol. 2021;23(6):865–6. https://doi.org/10.1093/neuonc/noab052.
14. Cimino PJ, Holland EC. Targeted copy number analysis outperforms histologic grading in predicting patient survival for WHO grades II/III IDH-mutant astrocytomas. Neuro Oncol. 2019;21(6):819–21. https://doi.org/10.1093/neuonc/noz052.
15. Reis GF, et al. CDKN2A loss is associated with shortened overall survival in lower-grade (world health organization grades II-III) astrocytomas. J Neuropathol Exp Neurol. 2015;74(5):442–52. https://doi.org/10.1097/nen.0000000000000188.
16. Shirahata M, et al. Novel, improved grading system(s) for IDH-mutant astrocytic gliomas. Acta Neuropathol. 2018;136(1):153–66. https://doi.org/10.1007/s00401-018-1849-4.
17. Chen W, et al. Novel insight into histological and molecular astrocytoma, IDH-mutant, Grade 4 by the updated WHO classification of central nervous system tumors. Cancer Med. 2023;12(18):18666–78. https://doi.org/10.1002/cam4.6476.
18. E. Calabrese *et al.* The University of California San Francisco Preoperative Diffuse Glioma MRI (UCSF-PDGM) (Version 4) . The Cancer Imaging Archive.
19. Jiang H, et al. 1p/19q codeletion and IDH1/2 mutation identified a subtype of anaplastic oligoastrocytomas with prognosis as favorable as anaplastic oligodendrogliomas. Neuro Oncol. 2013;15(6):775–82. https://doi.org/10.1093/neuonc/not027.
20. Jiang H, et al. A new prognostic scoring scale for patients with primary WHO grade III gliomas based on molecular predictors. J Neurooncol. 2013;111(3):367–75. https://doi.org/10.1007/s11060-012-1026-x.
21. Jiang H, Ren X, Zhang Z, Zeng W, Wang J, Lin S. Polysomy of chromosomes 1 and 19: an underestimated prognostic factor in oligodendroglial tumors. J Neurooncol. 2014;120(1):131–8. https://doi.org/10.1007/s11060-014-1526-y.
22. Jiang H, et al. Combination of immunotherapy and radiotherapy for recurrent malignant gliomas: results from a prospective study. Front Immunol. 2021;12:632547. https://doi.org/10.3389/fimmu.2021.632547.
23. Li M, et al. Combining MGMT promoter pyrosequencing and protein expression to optimize prognosis stratification in glioblastoma. Cancer Sci. 2021;112(9):3699–710. https://doi.org/10.1111/cas.15024.
24. Karschnia P, et al. Surgical management and outcome of newly diagnosed glioblastoma without contrast enhancement (low-grade appearance): a report of the RANO resect group. Neuro Oncol. 2024;26(1):166–77. https://doi.org/10.1093/neuonc/noad160.
25. Karschnia P, et al. Prognostic evaluation of re-resection for recurrent glioblastoma using the novel RANO classification for extent of resection: a report of the RANO resect group. Neuro Oncol. 2023;25(9):1672–85. https://doi.org/10.1093/neuonc/noad074.
26. Karschnia P, et al. Prognostic validation of a new classification system for extent of resection in glioblastoma: a report of the RANO resect group. Neuro Oncol. 2023;25(5):940–54. https://doi.org/10.1093/neuonc/noac193.
27. Lim DA, et al. Relationship of glioblastoma multiforme to neural stem cell regions predicts invasive and multifocal tumor phenotype. Neuro Oncol. 2007;9(4):424–9. https://doi.org/10.1215/15228517-2007-023.
28. Wen PY, et al. Updated response assessment criteria for high-grade gliomas: response assessment in neuro-oncology working group. J Clin Oncol. 2010;28(11):1963–72. https://doi.org/10.1200/jco.2009.26.3541.
29. Yang Y, et al. An analysis of 170 glioma patients and systematic review to investigate the association between IDH-1 mutations and preoperative glioma-related epilepsy. J Clin Neurosci. 2016;31:56–62. https://doi.org/10.1016/j.jocn.2015.11.030.
30. Michiwaki Y, et al. Relevance of calcification and contrast enhancement pattern for molecular diagnosis and survival prediction of gliomas based on the 2016 world health organization classification. Clin Neurol Neurosurg. 2019;187:105556. https://doi.org/10.1016/j.clineuro.2019.105556.
31. Nam YK, et al. Reproducible imaging-based prediction of molecular subtype and risk stratification of gliomas across different experience levels using a structured reporting system. Eur Radiol. 2021;31(10):7374–85. https://doi.org/10.1007/s00330-021-08015-4.
32. Mesny E, et al. Gyriform infiltration as imaging biomarker for molecular glioblastomas. J Neurooncol. 2022;157(3):511–21. https://doi.org/10.1007/s11060-022-03995-9.
33. Liu Y, et al. IDH-mutant grade 4 astrocytoma: a comparison integrating the clinical, pathological, and survival features between primary and secondary patients. J Neurosurg. 2024;140(1):94–103. https://doi.org/10.3171/2023.5.Jns222658.
34. Carrillo JA, et al. Relationship between tumor enhancement, edema, IDH1 mutational status, MGMT promoter methylation, and survival in glioblastoma. AJNR Am J Neuroradiol. 2012;33(7):1349–55. https://doi.org/10.3174/ajnr.A2950.
35. Lasocki A, Gaillard F, Tacey M, Drummond K, Stuckey S. Morphologic patterns of noncontrast-enhancing tumor in glioblastoma correlate with IDH1 mutation status and patient survival. J Clin Neurosci. 2018;47:168–73. https://doi.org/10.1016/j.jocn.2017.09.007.
36. Patel SH, et al. Fluid attenuation in non-contrast-enhancing tumor (nCET): an MRI marker for isocitrate dehydrogenase (IDH) mutation in glioblastoma. J Neurooncol. 2021;152(3):523–31. https://doi.org/10.1007/s11060-021-03720-y.
37. Wang K, et al. Radiological features combined with IDH1 status for predicting the survival outcome of glioblastoma patients. Neuro Oncol. 2016;18(4):589–97. https://doi.org/10.1093/neuonc/nov239.
38. Korshunov A, et al. Integrated molecular characterization of IDH-mutant glioblastomas. Neuropathol Appl Neurobiol. 2019;45(2):108–18. https://doi.org/10.1111/nan.12523.
39. Wong QH, et al. Molecular landscape of IDH-mutant primary astrocytoma grade IV/glioblastomas. Mod Pathol. 2021;34(7):1245–60. https://doi.org/10.1038/s41379-021-00778-x.